Methods and results of a search for gravitational waves associated with gamma-ray bursts using the GEO 600, LIGO, and Virgo detectors

J. Aasi,[1] B. P. Abbott,[1] R. Abbott,[1] T. Abbott,[2] M. R. Abernathy,[1] F. Acernese,[3,4] K. Ackley,[5] C. Adams,[6] T. Adams,[7] P. Addesso,[8] R. X. Adhikari,[1] C. Affeldt,[9] M. Agathos,[10] N. Aggarwal,[11] O. D. Aguiar,[12] P. Ajith,[13] A. Alemic,[14] B. Allen,[9,15,16] A. Allocca,[17,18] D. Amariutei,[5] M. Andersen,[19] R. A. Anderson,[1] S. B. Anderson,[1] W. G. Anderson,[15] K. Arai,[1] M. C. Araya,[1] C. Arceneaux,[20] J. S. Areeda,[21] S. Ast,[16] S. M. Aston,[6] P. Astone,[22] P. Aufmuth,[16] H. Augustus,[23] C. Aulbert,[9] B. E. Aylott,[23] S. Babak,[24] P. T. Baker,[25] G. Ballardin,[26] S. W. Ballmer,[14] J. C. Barayoga,[1] M. Barbet,[5] B. C. Barish,[1] D. Barker,[27] F. Barone,[3,4] B. Barr,[28] L. Barsotti,[11] M. Barsuglia,[29] M. A. Barton,[27] I. Bartos,[30] R. Bassiri,[19] A. Basti,[31,18] J. C. Batch,[27] J. Bauchrowitz,[9] Th. S. Bauer,[10] C. Baune,[9] V. Bavigadda,[26] B. Behnke,[24] M. Bejger,[32] M. G. Beker,[10] C. Belczynski,[33] A. S. Bell,[28] C. Bell,[28] G. Bergmann,[9] D. Bersanetti,[34,35] A. Bertolini,[10] J. Betzwieser,[6] I. A. Bilenko,[36] G. Billingsley,[1] J. Birch,[6] S. Biscans,[11] M. Bitossi,[18] C. Biwer,[14] M. A. Bizouard,[37] E. Black,[1] J. K. Blackburn,[1] L. Blackburn,[38] D. Blair,[39] S. Bloemen,[10,40] O. Bock,[9] T. P. Bodiya,[11] M. Boer,[41] G. Bogaert,[41] C. Bogan,[9] C. Bond,[23] F. Bondu,[42] L. Bonelli,[31,18] R. Bonnand,[43] R. Bork,[1] M. Born,[9] V. Boschi,[18] Sukanta Bose,[44,45] L. Bosi,[46] C. Bradaschia,[18] P. R. Brady,[15,47] V. B. Braginsky,[36] M. Branchesi,[48,49] J. E. Brau,[50] T. Briant,[51] D. O. Bridges,[6] A. Brillet,[41] M. Brinkmann,[9] V. Brisson,[37] A. F. Brooks,[1] D. A. Brown,[14] D. D. Brown,[23] F. Brückner,[23] S. Buchman,[19] A. Buikema,[11] T. Bulik,[33] H. J. Bulten,[52,10] A. Buonanno,[53] R. Burman,[39] D. Buskulic,[43] C. Buy,[29] L. Cadonati,[54,7] G. Cagnoli,[55] J. Cain,[20] J. Calderón Bustillo,[56] E. Calloni,[57,4] J. B. Camp,[38] P. Campsie,[28] K. C. Cannon,[58] B. Canuel,[26] J. Cao,[59] C. D. Capano,[53] F. Carbognani,[26] L. Carbone,[23] S. Caride,[60] G. Castaldi,[8] S. Caudill,[15] M. Cavaglià,[20] F. Cavalier,[37] R. Cavalieri,[26] C. Celerier,[19] G. Cella,[18] C. Cepeda,[1] E. Cesarini,[61] R. Chakraborty,[1] T. Chalermsongsak,[1] S. J. Chamberlin,[15] S. Chao,[62] P. Charlton,[63] E. Chassande-Mottin,[29] X. Chen,[39] Y. Chen,[64] A. Chincarini,[35] A. Chiummo,[26] H. S. Cho,[65] M. Cho,[53] J. H. Chow,[66] N. Christensen,[67] Q. Chu,[39] S. S. Y. Chua,[66] S. Chung,[39] G. Ciani,[5] F. Clara,[27] D. E. Clark,[19] J. A. Clark,[54] J. H. Clayton,[15] F. Cleva,[41] E. Coccia,[68,69] P.-F. Cohadon,[51] A. Colla,[70,22] C. Collette,[71] M. Colombini,[46] L. Cominsky,[72] M. Constancio, Jr.,[12] A. Conte,[70,22] D. Cook,[27] T. R. Corbitt,[2] N. Cornish,[25] A. Corsi,[73] C. A. Costa,[12] M. W. Coughlin,[74] J.-P. Coulon,[41] S. Countryman,[30] P. Couvares,[14] D. M. Coward,[39] M. J. Cowart,[6] D. C. Coyne,[1] R. Coyne,[73] K. Craig,[28] J. D. E. Creighton,[15] R. P. Croce,[8] S. G. Crowder,[75] A. Cumming,[28] L. Cunningham,[28] E. Cuoco,[26] C. Cutler,[64] K. Dahl,[9] T. Dal Canton,[9] M. Damjanic,[9] S. L. Danilishin,[39] S. D'Antonio,[61] K. Danzmann,[16,9] V. Dattilo,[26] H. Daveloza,[76] M. Davier,[37] G. S. Davies,[28] E. J. Daw,[77] R. Day,[26] T. Dayanga,[44] D. DeBra,[19] G. Debreczeni,[78] J. Degallaix,[55] S. Deléglise,[51] W. Del Pozzo,[23] W. Del Pozzo,[10] T. Denker,[9] T. Dent,[9] H. Dereli,[41] V. Dergachev,[1] R. De Rosa,[57,4] R. T. DeRosa,[2] R. DeSalvo,[8] S. Dhurandhar,[45] M. Díaz,[76] J. Dickson,[66] L. Di Fiore,[4] A. Di Lieto,[31,18] I. Di Palma,[9] A. Di Virgilio,[18] V. Dolique,[55] E. Dominguez,[79] F. Donovan,[11] K. L. Dooley,[9] S. Doravari,[6] R. Douglas,[28] T. P. Downes,[15] M. Drago,[80,81] R. W. P. Drever,[1] J. C. Driggers,[1] Z. Du,[59] M. Ducrot,[43] S. Dwyer,[27] T. Eberle,[9] T. Edo,[77] M. Edwards,[7] A. Effler,[2] H.-B. Eggenstein,[9] P. Ehrens,[1] J. Eichholz,[5] S. S. Eikenberry,[5] G. Endrőczi,[78] R. Essick,[11] T. Etzel,[1] M. Evans,[11] T. Evans,[6] M. Factourovich,[30] V. Fafone,[68,61] S. Fairhurst,[7] X. Fan,[28] Q. Fang,[39] S. Farinon,[35] B. Farr,[82] W. M. Farr,[23] M. Favata,[83] D. Fazi,[82] H. Fehrmann,[9] M. M. Fejer,[19] D. Feldbaum,[5,6] F. Feroz,[74] I. Ferrante,[31,18] E. C. Ferreira,[12] F. Ferrini,[26] F. Fidecaro,[31,18] L. S. Finn,[84] I. Fiori,[26] R. P. Fisher,[14] R. Flaminio,[55] N. Fotopoulos,[1] J.-D. Fournier,[41] S. Franco,[37] S. Frasca,[70,22] F. Frasconi,[18] M. Frede,[9] Z. Frei,[85] A. Freise,[23] R. Frey,[50] T. T. Fricke,[9] P. Fritschel,[11] V. V. Frolov,[6] P. Fulda,[5] M. Fyffe,[6] J. R. Gair,[74] L. Gammaitoni,[86,46] S. Gaonkar,[45] F. Garufi,[57,4] N. Gehrels,[38] G. Gemme,[35] B. Gendre,[41] E. Genin,[26] A. Gennai,[18] S. Ghosh,[10,40] J. A. Giaime,[6,2] K. D. Giardina,[6] A. Giazotto,[18] C. Gill,[28] J. Gleason,[5] E. Goetz,[9] R. Goetz,[5] L. Gondan,[85] G. González,[2] N. Gordon,[28] M. L. Gorodetsky,[36] S. Gossan,[64] S. Goßler,[9] R. Gouaty,[43] C. Gräf,[28] P. B. Graff,[38] M. Granata,[55] A. Grant,[28] S. Gras,[11] C. Gray,[27] R. J. S. Greenhalgh,[87] A. M. Gretarsson,[88] P. Groot,[40] H. Grote,[9] K. Grover,[23] S. Grunewald,[24] G. M. Guidi,[48,49] C. J. Guido,[6] K. Gushwa,[1] E. K. Gustafson,[1] R. Gustafson,[60] J. Ha,[89] E. D. Hall,[1] W. Hamilton,[2] D. Hammer,[15] G. Hammond,[28] M. Hanke,[9] J. Hanks,[27] C. Hanna,[90,84] M. D. Hannam,[7] J. Hanson,[6] K. Haris,[98] J. Harms,[1] G. M. Harry,[91] I. W. Harry,[14] E. D. Harstad,[50] M. Hart,[28] M. T. Hartman,[5] C.-J. Haster,[23] K. Haughian,[28] A. Heidmann,[51] M. Heintze,[5,6] H. Heitmann,[41] P. Hello,[37] G. Hemming,[26] M. Hendry,[28] I. S. Heng,[28] A. W. Heptonstall,[1] M. Heurs,[9] M. Hewitson,[9] S. Hild,[28] D. Hoak,[54] K. A. Hodge,[1] D. Hofman,[55] K. Holt,[6] P. Hopkins,[7] T. Horrom,[92] D. Hoske,[93] D. J. Hosken,[93] J. Hough,[28] E. J. Howell,[39] Y. Hu,[28] E. Huerta,[14] B. Hughey,[88] S. Husa,[56] S. H. Huttner,[28] M. Huynh,[15] T. Huynh-Dinh,[6] A. Idrisy,[84] D. R. Ingram,[27] R. Inta,[84] G. Islas,[21] T. Isogai,[11] A. Ivanov,[1] B. R. Iyer,[94] K. Izumi,[27] M. Jacobson,[1] H. Jang,[95] P. Jaranowski,[96] Y. Ji,[59] F. Jiménez-Forteza,[56] W. W. Johnson,[2] D. I. Jones,[97] G. Jones,[7] R. Jones,[28] R. J. G. Jonker,[10] L. Ju,[39] P. Kalmus,[1] V. Kalogera,[82] S. Kandhasamy,[20] G. Kang,[95] J. B. Kanner,[1] J. Karlen,[54] M. Kasprzack,[37,26] E. Katsavounidis,[11] W. Katzman,[6] H. Kaufer,[16] S. Kaufer,[16] T. Kaur,[39] K. Kawabe,[27] F. Kawazoe,[9] F. Kéfélian,[41] G. M. Keiser,[19] D. Keitel,[9] D. B. Kelley,[14] W. Kells,[1] D. G. Keppel,[9] A. Khalaidovski,[9] F. Y. Khalili,[36] E. A. Khazanov,[99] C. Kim,[89,95] K. Kim,[100] N. G. Kim,[95] N. Kim,[19] S. Kim,[95] Y.-M. Kim,[65] E. J. King,[93] P. J. King,[1] D. L. Kinzel,[6] J. S. Kissel,[27] S. Klimenko,[5]

J. Kline,[15] S. Koehlenbeck,[9] K. Kokeyama,[2] V. Kondrashov,[1] S. Koranda,[15] W. Z. Korth,[1] I. Kowalska,[33] D. B. Kozak,[1] V. Kringel,[9] B. Krishnan,[9] A. Królak,[101,102] G. Kuehn,[9] A. Kumar,[103] D. Nanda Kumar,[5] P. Kumar,[14] R. Kumar,[28] L. Kuo,[62] A. Kutynia,[101] P. K. Lam,[66] M. Landry,[27] B. Lantz,[19] S. Larson,[82] P. D. Lasky,[104] C. Lazzaro,[105] P. Leaci,[24] S. Leavey,[28] E. O. Lebigot,[59] C. H. Lee,[65] H. K. Lee,[100] H. M. Lee,[89] J. Lee,[100] P. J. Lee,[11] M. Leonardi,[80,81] J. R. Leong,[9] A. Le Roux,[6] N. Leroy,[37] N. Letendre,[43] Y. Levin,[106] B. Levine,[27] J. Lewis,[1] T. G. F. Li,[1] K. Libbrecht,[1] A. Libson,[11] A. C. Lin,[19] T. B. Littenberg,[82] N. A. Lockerbie,[107] V. Lockett,[21] D. Lodhia,[23] K. Loew,[88] J. Logue,[28] A. L. Lombardi,[54] E. Lopez,[108] M. Lorenzini,[68,61] V. Loriette,[109] M. Lormand,[6] G. Losurdo,[49] J. Lough,[14] M. J. Lubinski,[27] H. Lück,[16,9] A. P. Lundgren,[9] Y. Ma,[39] E. P. Macdonald,[7] T. MacDonald,[19] B. Machenschalk,[9] M. MacInnis,[11] D. M. Macleod,[2] F. Magaña-Sandoval,[14] R. Magee,[44] M. Mageswaran,[1] C. Maglione,[79] K. Mailand,[1] E. Majorana,[22] I. Maksimovic,[109] V. Malvezzi,[68,61] N. Man,[41] G. M. Manca,[9] I. Mandel,[23] V. Mandic,[75] V. Mangano,[70,22] N. M. Mangini,[54] G. Mansell,[66] M. Mantovani,[18] F. Marchesoni,[110,46] F. Marion,[43] S. Márka,[30] Z. Márka,[30] A. Markosyan,[19] E. Maros,[1] J. Marque,[26] F. Martelli,[48,49] I. W. Martin,[28] R. M. Martin,[5] L. Martinelli,[41] D. Martynov,[1] J. N. Marx,[1] K. Mason,[11] A. Masserot,[43] T. J. Massinger,[14] F. Matichard,[11] L. Matone,[30] N. Mavalvala,[11] G. May,[2] N. Mazumder,[98] G. Mazzolo,[9] R. McCarthy,[27] D. E. McClelland,[66] S. C. McGuire,[111] G. McIntyre,[1] J. McIver,[54] K. McLin,[72] D. Meacher,[41] G. D. Meadors,[60] M. Mehmet,[9] J. Meidam,[10] M. Meinders,[16] A. Melatos,[104] G. Mendell,[27] R. A. Mercer,[15] S. Meshkov,[1] C. Messenger,[28] A. Meyer,[54] M. S. Meyer,[6] P. M. Meyers,[75] F. Mezzani,[22,70] H. Miao,[64] C. Michel,[55] E. E. Mikhailov,[92] L. Milano,[57,4] J. Miller,[11] Y. Minenkov,[61] C. M. F. Mingarelli,[23] C. Mishra,[98] S. Mitra,[45] V. P. Mitrofanov,[36] G. Mitselmakher,[5] R. Mittleman,[11] B. Moe,[15] A. Moggi,[18] M. Mohan,[26] S. R. P. Mohapatra,[14] D. Moraru,[27] G. Moreno,[27] N. Morgado,[55] S. R. Morriss,[76] K. Mossavi,[9] B. Mours,[43] C. M. Mow-Lowry,[9] C. L. Mueller,[5] G. Mueller,[5] S. Mukherjee,[76] A. Mullavey,[2] J. Munch,[93] D. Murphy,[30] P. G. Murray,[28] A. Mytidis,[5] M. F. Nagy,[78] I. Nardecchia,[68,61] L. Naticchioni,[70,22] R. K. Nayak,[112] V. Necula,[5] G. Nelemans,[10,40] I. Neri,[86,46] M. Neri,[34,35] G. Newton,[28] T. Nguyen,[66] A. B. Nielsen,[9] S. Nissanke,[64] A. H. Nitz,[14] F. Nocera,[26] D. Nolting,[6] M. E. N. Normandin,[76] L. K. Nuttall,[15] E. Ochsner,[15] J. O'Dell,[87] E. Oelker,[11] J. J. Oh,[113] S. H. Oh,[113] F. Ohme,[7] S. Omar,[19] P. Oppermann,[9] R. Oram,[6] B. O'Reilly,[6] W. Ortega,[79] R. O'Shaughnessy,[15] C. Osthelder,[1] D. J. Ottaway,[93] R. S. Ottens,[5] H. Overmier,[6] B. J. Owen,[84] C. Padilla,[21] A. Pai,[98] O. Palashov,[99] C. Palomba,[22] H. Pan,[62] Y. Pan,[53] C. Pankow,[15] F. Paoletti,[26,18] M. A. Papa,[15,24] H. Paris,[19] A. Pasqualetti,[26] R. Passaquieti,[31,18] D. Passuello,[18] P. Patel,[1] M. Pedraza,[1] A. Pele,[27] S. Penn,[114] A. Perreca,[14] M. Phelps,[1] M. Pichot,[41] M. Pickenpack,[9] F. Piergiovanni,[48,49] V. Pierro,[8] L. Pinard,[55] I. M. Pinto,[8] M. Pitkin,[28] J. Poeld,[9] R. Poggiani,[31,18] A. Poteomkin,[99] J. Powell,[28] J. Prasad,[45] V. Predoi,[7] S. Premachandra,[106] T. Prestegard,[75] L. R. Price,[1] M. Prijatelj,[26] S. Privitera,[1] G. A. Prodi,[80,81] L. Prokhorov,[36] O. Puncken,[76] M. Punturo,[46] P. Puppo,[22] M. Pürrer,[7] J. Qin,[39] V. Quetschke,[76] E. Quintero,[1] R. Quitzow-James,[50] F. J. Raab,[27] D. S. Rabeling,[52,10] I. Rácz,[78] H. Radkins,[27] P. Raffai,[85] S. Raja,[115] G. Rajalakshmi,[116] M. Rakhmanov,[76] C. Ramet,[6] K. Ramirez,[76] P. Rapagnani,[70,22] V. Raymond,[1] M. Razzano,[31,18] V. Re,[68,61] S. Recchia,[68,69] C. M. Reed,[27] T. Regimbau,[41] S. Reid,[117] D. H. Reitze,[1,5] O. Reula,[79] E. Rhoades,[88] F. Ricci,[70,22] R. Riesen,[6] K. Riles,[60] N. A. Robertson,[1,28] F. Robinet,[37] A. Rocchi,[61] S. B. Roddy,[6] S. Rogstad,[54] L. Rolland,[43] J. G. Rollins,[1] R. Romano,[3,4] G. Romanov,[92] J. H. Romie,[6] D. Rosińska,[118,32] S. Rowan,[28] A. Rüdiger,[9] P. Ruggi,[26] K. Ryan,[27] F. Salemi,[9] L. Sammut,[104] V. Sandberg,[27] J. R. Sanders,[60] S. Sankar,[11] V. Sannibale,[1] I. Santiago-Prieto,[28] E. Saracco,[55] B. Sassolas,[55] B. S. Sathyaprakash,[7] P. R. Saulson,[14] R. Savage,[27] J. Scheuer,[82] R. Schilling,[9] M. Schilman,[79] P. Schmidt,[7] R. Schnabel,[9,16] R. M. S. Schofield,[50] E. Schreiber,[9] D. Schuette,[9] B. F. Schutz,[7,24] J. Scott,[28] S. M. Scott,[66] D. Sellers,[6] A. S. Sengupta,[119] D. Sentenac,[26] V. Sequino,[68,61] A. Sergeev,[99] D. A. Shaddock,[66] S. Shah,[10,40] M. S. Shahriar,[82] M. Shaltev,[9] Z. Shao,[1] B. Shapiro,[19] P. Shawhan,[53] D. H. Shoemaker,[11] T. L. Sidery,[23] K. Siellez,[41] X. Siemens,[15] D. Sigg,[27] D. Simakov,[9] A. Singer,[1] L. Singer,[1] R. Singh,[2] A. M. Sintes,[56] B. J. J. Slagmolen,[66] J. Slutsky,[38] J. R. Smith,[21] M. R. Smith,[1] R. J. E. Smith,[1] N. D. Smith-Lefebvre,[1] E. J. Son,[113] B. Sorazu,[28] T. Souradeep,[45] A. Staley,[30] J. Stebbins,[19] J. Steinlechner,[9,28] S. Steinlechner,[9,28] B. C. Stephens,[15] S. Steplewski,[44] S. Stevenson,[23] R. Stone,[76] D. Stops,[23] K. A. Strain,[28] N. Straniero,[55] S. Strigin,[36] R. Sturani,[120] A. L. Stuver,[6] T. Z. Summerscales,[121] S. Susmithan,[39] P. J. Sutton,[7] B. Swinkels,[26] M. Tacca,[29] D. Talukder,[50] D. B. Tanner,[5] J. Tao,[2] S. P. Tarabrin,[9] R. Taylor,[1] G. Tellez,[76] M. P. Thirugnanasambandam,[1] M. Thomas,[6] P. Thomas,[27] K. A. Thorne,[6] K. S. Thorne,[64] E. Thrane,[1] V. Tiwari,[5] K. V. Tokmakov,[107] C. Tomlinson,[77] M. Tonelli,[31,18] C. V. Torres,[76] C. I. Torrie,[1,28] F. Travasso,[86,46] G. Traylor,[6] M. Trias,[56] M. Tse,[30] D. Tshilumba,[71] H. Tuennermann,[9] D. Ugolini,[122] C. S. Unnikrishnan,[116] A. L. Urban,[15] S. A. Usman,[14] H. Vahlbruch,[16] G. Vajente,[31,18] G. Valdes,[76] M. Vallisneri,[64] M. van Beuzekom,[10] J. F. J. van den Brand,[52,10] C. Van Den Broeck,[10] M. V. van der Sluys,[10,40] J. van Heijningen,[10] A. A. van Veggel,[28] S. Vass,[1] M. Vasúth,[78] R. Vaulin,[11] A. Vecchio,[23] G. Vedovato,[105] J. Veitch,[10] P. J. Veitch,[93] K. Venkateswara,[123] D. Verkindt,[43] F. Vetrano,[48,49] A. Viceré,[48,49] R. Vincent-Finley,[111] J.-Y. Vinet,[41] S. Vitale,[11] T. Vo,[27] H. Vocca,[86,46] C. Vorvick,[27] W. D. Vousden,[23] S. P. Vyachanin,[36] A. R. Wade,[66] L. Wade,[15] M. Wade,[15] M. Walker,[2] L. Wallace,[1] S. Walsh,[15] M. Wang,[23] X. Wang,[59] R. L. Ward,[66] M. Was,[9] B. Weaver,[27] L.-W. Wei,[41] M. Weinert,[9] A. J. Weinstein,[1] R. Weiss,[11] T. Welborn,[6] L. Wen,[39] P. Wessels,[9] M. West,[14] T. Westphal,[9] K. Wette,[9] J. T. Whelan,[124] D. J. White,[77] B. F. Whiting,[5] K. Wiesner,[9] C. Wilkinson,[27] K. Williams,[111] L. Williams,[5] R. Williams,[1] T. D. Williams,[125]

A. R. Williamson,[7] J. L. Willis,[126] B. Willke,[16,9] M. Wimmer,[9] W. Winkler,[9] C. C. Wipf,[11] A. G. Wiseman,[15] H. Wittel,[9] G. Woan,[28] N. Wolovick,[79] J. Worden,[27] Y. Wu,[5] J. Yablon,[82] I. Yakushin,[6] W. Yam,[11] H. Yamamoto,[1] C. C. Yancey,[53] H. Yang,[64] S. Yoshida,[125] M. Yvert,[43] A. Zadrożny,[101] M. Zanolin,[88] J.-P. Zendri,[105] Fan Zhang,[11,59] L. Zhang,[1] C. Zhao,[39] H. Zhu,[84] X. J. Zhu,[39] M. E. Zucker,[11] S. Zuraw,[54] and J. Zweizig[1]

(LIGO Scientific Collaboration and Virgo Collaboration)

[1]LIGO, California Institute of Technology, Pasadena, California 91125, USA
[2]Louisiana State University, Baton Rouge, Louisiana 70803, USA
[3]Università di Salerno, Fisciano, I-84084 Salerno, Italy
[4]INFN, Sezione di Napoli, Complesso Universitario di Monte S.Angelo, I-80126 Napoli, Italy
[5]University of Florida, Gainesville, Florida 32611, USA
[6]LIGO Livingston Observatory, Livingston, Louisiana 70754, USA
[7]Cardiff University, Cardiff, CF24 3AA, United Kingdom
[8]University of Sannio at Benevento, I-82100 Benevento, Italy,
and INFN, Sezione di Napoli, I-80100 Napoli, Italy
[9]Albert-Einstein-Institut, Max-Planck-Institut für Gravitationsphysik, D-30167 Hannover, Germany
[10]Nikhef, Science Park, 1098 XG Amsterdam, The Netherlands
[11]LIGO, Massachusetts Institute of Technology, Cambridge, Massachusetts 02139, USA
[12]Instituto Nacional de Pesquisas Espaciais, 12227-010 - São José dos Campos, SP, Brazil
[13]International Centre for Theoretical Sciences, Tata Institute of Fundamental Research,
Bangalore 560012, India
[14]Syracuse University, Syracuse, New York 13244, USA
[15]University of Wisconsin–Milwaukee, Milwaukee, Wisconsin 53201, USA
[16]Leibniz Universität Hannover, D-30167 Hannover, Germany
[17]Università di Siena, I-53100 Siena, Italy
[18]INFN, Sezione di Pisa, I-56127 Pisa, Italy
[19]Stanford University, Stanford, California 94305, USA
[20]The University of Mississippi, University, Mississippi 38677, USA
[21]California State University Fullerton, Fullerton, California 92831, USA
[22]INFN, Sezione di Roma, I-00185 Roma, Italy
[23]University of Birmingham, Birmingham, B15 2TT, United Kingdom
[24]Albert-Einstein-Institut, Max-Planck-Institut für Gravitationsphysik, D-14476 Golm, Germany
[25]Montana State University, Bozeman, Montana 59717, USA
[26]European Gravitational Observatory (EGO), I-56021 Cascina, Pisa, Italy
[27]LIGO Hanford Observatory, Richland, Washington 99352, USA
[28]SUPA, University of Glasgow, Glasgow, G12 8QQ, United Kingdom
[29]APC, AstroParticule et Cosmologie, Université Paris Diderot, CNRS/IN2P3, CEA/Irfu, Observatoire de
Paris, Sorbonne Paris Cité, 10, rue Alice Domon et Léonie Duquet, F-75205 Paris Cedex 13, France
[30]Columbia University, New York, New York 10027, USA
[31]Università di Pisa, I-56127 Pisa, Italy
[32]CAMK-PAN, 00-716 Warsaw, Poland
[33]Astronomical Observatory Warsaw University, 00-478 Warsaw, Poland
[34]Università degli Studi di Genova, I-16146 Genova, Italy
[35]INFN, Sezione di Genova, I-16146 Genova, Italy
[36]Faculty of Physics, Lomonosov Moscow State University, Moscow 119991, Russia
[37]LAL, Université Paris-Sud, IN2P3/CNRS, F-91898 Orsay, France
[38]NASA/Goddard Space Flight Center, Greenbelt, Maryland 20771, USA
[39]University of Western Australia, Crawley, WA 6009, Australia
[40]Department of Astrophysics/IMAPP, Radboud University Nijmegen,
P.O. Box 9010, 6500 GL Nijmegen, The Netherlands
[41]Université Nice-Sophia-Antipolis, CNRS, Observatoire de la Côte d'Azur, F-06304 Nice, France
[42]Institut de Physique de Rennes, CNRS, Université de Rennes 1, F-35042 Rennes, France
[43]Laboratoire d'Annecy-le-Vieux de Physique des Particules (LAPP), Université de Savoie,
CNRS/IN2P3, F-74941 Annecy-le-Vieux, France
[44]Washington State University, Pullman, Washington 99164, USA
[45]Inter-University Centre for Astronomy and Astrophysics, Pune - 411007, India
[46]INFN, Sezione di Perugia, I-06123 Perugia, Italy
[47]Yukawa Institute for Theoretical Physics, Kyoto University, Kyoto 606-8502, Japan
[48]Università degli Studi di Urbino 'Carlo Bo', I-61029 Urbino, Italy

[49]*INFN, Sezione di Firenze, I-50019 Sesto Fiorentino, Firenze, Italy*

[50]*University of Oregon, Eugene, Oregon 97403, USA*

[51]*Laboratoire Kastler Brossel, ENS, CNRS, UPMC, Université Pierre et Marie Curie, F-75005 Paris, France*

[52]*VU University Amsterdam, 1081 HV Amsterdam, The Netherlands*

[53]*University of Maryland, College Park, Maryland 20742, USA*

[54]*University of Massachusetts Amherst, Amherst, Massachusetts 01003, USA*

[55]*Laboratoire des Matériaux Avancés (LMA), IN2P3/CNRS, Université de Lyon, F-69622 Villeurbanne, Lyon, France*

[56]*Universitat de les Illes Balears, E-07122 Palma de Mallorca, Spain*

[57]*Università di Napoli 'Federico II', Complesso Universitario di Monte S.Angelo, I-80126 Napoli, Italy*

[58]*Canadian Institute for Theoretical Astrophysics, University of Toronto, Toronto, Ontario, M5 S 3H8, Canada*

[59]*Tsinghua University, Beijing 100084, China*

[60]*University of Michigan, Ann Arbor, Michigan 48109, USA*

[61]*INFN, Sezione di Roma Tor Vergata, I-00133 Roma, Italy*

[62]*National Tsing Hua University, Hsinchu Taiwan 300*

[63]*Charles Sturt University, Wagga Wagga, NSW 2678, Australia*

[64]*Caltech-CaRT, Pasadena, California 91125, USA*

[65]*Pusan National University, Busan 609-735, Korea*

[66]*Australian National University, Canberra, ACT 0200, Australia*

[67]*Carleton College, Northfield, Minnesota 55057, USA*

[68]*Università di Roma Tor Vergata, I-00133 Roma, Italy*

[69]*INFN, Gran Sasso Science Institute, I-67100 L'Aquila, Italy*

[70]*Università di Roma 'La Sapienza', I-00185 Roma, Italy*

[71]*University of Brussels, Brussels 1050 Belgium*

[72]*Sonoma State University, Rohnert Park, California 94928, USA*

[73]*The George Washington University, Washington, DC 20052, USA*

[74]*University of Cambridge, Cambridge, CB2 1TN, United Kingdom*

[75]*University of Minnesota, Minneapolis, Minnesota 55455, USA*

[76]*The University of Texas at Brownsville, Brownsville, Texas 78520, USA*

[77]*The University of Sheffield, Sheffield S10 2TN, United Kingdom*

[78]*Wigner RCP, RMKI, H-1121 Budapest, Konkoly Thege Miklós út 29-33, Hungary*

[79]*Argentinian Gravitational Wave Group, Cordoba Cordoba 5000, Argentina*

[80]*Università di Trento, I-38050 Povo, Trento, Italy*

[81]*INFN, Gruppo Collegato di Trento, I-38050 Povo, Trento, Italy*

[82]*Northwestern University, Evanston, Illinois 60208, USA*

[83]*Montclair State University, Montclair, New Jersey 07043, USA*

[84]*The Pennsylvania State University, University Park, Pennsylvania 16802, USA*

[85]*MTA Eötvös University, 'Lendulet' A. R. G., Budapest 1117, Hungary*

[86]*Università di Perugia, I-06123 Perugia, Italy*

[87]*Rutherford Appleton Laboratory, HSIC, Chilton, Didcot, Oxon, OX11 0QX, United Kingdom*

[88]*Embry-Riddle Aeronautical University, Prescott, Arizona 86301, USA*

[89]*Seoul National University, Seoul 151-742, Korea*

[90]*Perimeter Institute for Theoretical Physics, Waterloo, Ontario, N2 L 2Y5, Canada*

[91]*American University, Washington, DC 20016, USA*

[92]*College of William and Mary, Williamsburg, Virginia 23187, USA*

[93]*University of Adelaide, Adelaide, SA 5005, Australia*

[94]*Raman Research Institute, Bangalore, Karnataka 560080, India*

[95]*Korea Institute of Science and Technology Information, Daejeon 305-806, Korea*

[96]*Biał ystok University, 15-424 Biał ystok, Poland*

[97]*University of Southampton, Southampton, SO17 1BJ, United Kingdom*

[98]*IISER-TVM, CET Campus, Trivandrum Kerala 695016, India*

[99]*Institute of Applied Physics, Nizhny Novgorod, 603950, Russia*

[100]*Hanyang University, Seoul 133-791, Korea*

[101]*NCBJ, 05-400 Świerk-Otwock, Poland*

[102]*IM-PAN, 00-956 Warsaw, Poland*

[103]*Institute for Plasma Research, Bhat, Gandhinagar 382428, India*

[104]*The University of Melbourne, Parkville, VIC 3010, Australia*

[105]*INFN, Sezione di Padova, I-35131 Padova, Italy*

[106]Monash University, Victoria 3800, Australia

[107]SUPA, University of Strathclyde, Glasgow, G1 1XQ, United Kingdom

[108]Louisiana Tech University, Ruston, Louisiana 71272, USA

[109]ESPCI, CNRS, F-75005 Paris, France

[110]Università di Camerino, Dipartimento di Fisica, I-62032 Camerino, Italy

[111]Southern University and A&M College, Baton Rouge, Louisiana 70813, USA

[112]IISER-Kolkata, Mohanpur, West Bengal 741252, India

[113]National Institute for Mathematical Sciences, Daejeon 305-390, Korea

[114]Hobart and William Smith Colleges, Geneva, New York 14456, USA

[115]RRCAT, Indore MP 452013, India

[116]Tata Institute for Fundamental Research, Mumbai 400005, India

[117]SUPA, University of the West of Scotland, Paisley, PA1 2BE, United Kingdom

[118]Institute of Astronomy, 65-265 Zielona Góra, Poland

[119]Indian Institute of Technology, Gandhinagar Ahmedabad Gujarat 382424, India

[120]Instituto de Física Teórica, Univ. Estadual Paulista/ICTP South American Institute for Fundamental Research, São Paulo SP 01140-070, Brazil

[121]Andrews University, Berrien Springs, Michigan 49104, USA

[122]Trinity University, San Antonio, Texas 78212, USA

[123]University of Washington, Seattle, Washington 98195, USA

[124]Rochester Institute of Technology, Rochester, New York 14623, USA

[125]Southeastern Louisiana University, Hammond, Louisiana 70402, USA

[126]Abilene Christian University, Abilene, Texas 79699, USA

In this paper we report on a search for short-duration gravitational wave bursts in the frequency range 64 Hz–1792 Hz associated with gamma-ray bursts (GRBs), using data from GEO 600 and one of the LIGO or Virgo detectors. We introduce the method of a linear search grid to analyze GRB events with large sky localization uncertainties, for example the localizations provided by the *Fermi* Gamma-ray Burst Monitor (GBM). Coherent searches for gravitational waves (GWs) can be computationally intensive when the GRB sky position is not well localized, due to the corrections required for the difference in arrival time between detectors. Using a linear search grid we are able to reduce the computational cost of the analysis by a factor of $\mathcal{O}(10)$ for GBM events. Furthermore, we demonstrate that our analysis pipeline can improve upon the sky localization of GRBs detected by the GBM, if a high-frequency GW signal is observed in coincidence. We use the method of the linear grid in a search for GWs associated with 129 GRBs observed satellite-based gamma-ray experiments between 2006 and 2011. The GRBs in our sample had not been previously analyzed for GW counterparts. A fraction of our GRB events are analyzed using data from GEO 600 while the detector was using squeezed-light states to improve its sensitivity; this is the first search for GWs using data from a squeezed-light interferometric observatory. We find no evidence for GW signals, either with any individual GRB in this sample or with the population as a whole. For each GRB we place lower bounds on the distance to the progenitor, under an assumption of a fixed GW emission energy of $10^{-2} \mathrm{M}\odot c^2$, with a median exclusion distance of 0.8 Mpc for emission at 500 Hz and 0.3 Mpc at 1 kHz. The reduced computational cost associated with a linear search grid will enable rapid searches for GWs associated with *Fermi* GBM events once the advanced LIGO and Virgo detectors begin operation.

I. INTRODUCTION

Gamma-ray bursts (GRBs) are intense flashes of high-energy photons which are observed approximately once per day and are distributed isotropically on the sky [1]. Since their public discovery in 1973 [2], it has been found that most GRBs occur at extragalactic distances, and there is growing evidence that they emit gamma-rays in tightly beamed relativistic jets [3,4]. GRBs are grouped into two broad classes based on their spectral hardness and the duration of the initial gamma-ray flash [5]. The progenitors of long-soft GRBs are generally accepted to be core-collapse supernovae (CCSN) in massive, rapidly rotating stars [6–8]. The progenitors of short-hard GRBs have yet to be definitively constrained by observation, but are widely thought to be associated with the mergers of binary neutron star or neutron star-black hole systems. Events of this sort are referred to as compact binary coalescences (CBCs) [9–16]. Both the CCSN and CBC scenarios result in the formation of a stellar-mass black hole or magnetar with an accretion disk. CBCs are expected to be bright sources of

gravitational waves (GWs), while the GW emission by CCSN is more speculative.

Although it is expected that most GRB progenitors will be at distances too large for any counterpart GW signals to be detectable by the current generation of observatories, it is possible that a few GRBs could be located nearby. The nondetection of GW counterparts to GRB 051103 [17] and GRB 070201 [18], which were short-duration GRBs with error boxes overlapping the M81 galaxy (at 3.6 Mpc) and the Andromeda galaxy (at 770 kpc), respectively, ruled out CBC progenitors in M81 or M31 with high confidence. Studies of long GRBs indicate the existence of a local population of underluminous events with an observed rate density approximately 10^3 times that of the high-luminosity population [19–24]. Approximately ~85% of the GRBs in our sample do not have measured redshifts, so it is possible that one or more events could be much closer than the typical ~Gpc distances of GRBs.

Previously, searches for GWs associated with GRBs were performed on approximately 500 GRBs which occurred during times when at least two of the LIGO and Virgo detectors were collecting data [17,18,25–27]. Related analyses have searched for extended-duration GW signals associated with long GRBs [28], and for GWs arising from the oscillation of neutron star f-modes in magnetars and soft gamma-ray repeaters [29–31]. Most recently, data from the fifth and sixth LIGO science runs (S5, S6) and the first, second and third Virgo science runs (VSR1, 2 and 3) were searched for short-duration GW bursts and for signals from CBCs, using GRB events detected by the InterPlanetary Network (IPN) [32]. No evidence for a signal was found in these searches.

The GEO 600 detector has its best sensitivity at frequencies greater than 500 Hz, and because of its limited sensitivity at low frequencies it was not included in previous searches. However, the high duty cycle of GEO 600 yields a substantial number of GRBs which occurred during times of joint observation with one of the LIGO/Virgo detectors. It is these GRBs which we consider here.

The central engines of GRBs are expected to emit GWs at frequencies above 500 Hz through a variety of mechanisms, although the amplitude of this emission is not well constrained by simulation. Coherent searches for high-frequency signals from GRBs can be computationally challenging when the uncertainty in the GRB sky location is very large, due to the shift in the arrival time of GW signals at widely separated detectors as the sky position varies across the error box. Previous searches for GWs associated with poorly localized GRBs have used a search band of 64-500 Hz, which preserves the detection efficiency of the search for the frequencies with the best detector sensitivity.

In this paper, we present the methods and results of a search for generic GW burst signals associated with 129 GRBs which were detected by satellite-based gamma-ray

experiments between February 4, 2006 and November 3, 2011, and occurred when GEO 600 and one other km-scale GW observatory were taking data. The search targets GW signals with durations $\lesssim 1$ s and frequencies between 64 Hz and 1792 Hz. Unlike previous GW searches that analyzed GRBs with large sky location uncertainty, we do not repeat the search across the entire GRB uncertainty region. Instead, we use a linear grid of search points to cover the uncertainty region in the direction of the maximum gradient of the time delay between the detectors. For a search using data from two widely separated GW observatories, this technique is sufficient to preserve the sensitivity of the analysis while reducing the computational cost of analyzing each GRB by a factor of ten or more.

This paper is organized in the following way. In Sec. II, we discuss possible GW signals associated with GRBs that are detectable given our analysis parameters. In Sec. III we describe the GW observatories whose data are used in the search. Section IV describes the methods of the search and the analysis procedure for GW signals, and in Sec. V we describe the sample of GRBs included in our search and present the results. Finally, in Sec. VI we summarize the analysis and discuss the application of these methods to searches in the era of advanced GW detectors.

II. MODELS FOR GW SIGNALS FROM GRB PROGENITORS

The progenitors of GRBs are expected to have characteristic GW signatures [33] depending on the physics of the GRB central engine. In this section we describe plausible models for GW emission from these systems, especially at high frequencies (>500 Hz) where this search is most sensitive.

Short GRBs are believed to be associated with the merger of a neutron star either with another neutron star or a black hole [34]. The inspiral phase of these mergers is expected to be a bright source of gravitational radiation [35]. While most of the GW energy flux from the inspiral occurs at frequencies below 500 Hz, numerical simulations of binary neutron star mergers have shown that substantial GW emission can occur at frequencies greater than 1 kHz [36,37]. Binary neutron star mergers may result in the formation of a hypermassive neutron star, which can produce strong GW emission as it collapses to a black hole [38,39].

Short GRBs with unknown redshifts could also be produced by giant flares from a local population of soft gamma-ray repeaters [40–43]. Sources of this kind are expected to produce some GW energy ($\lesssim 10^{-8} M_\odot c^2$) in the 1 kHz–2 kHz range [44–47].

The progenitors of long GRBs are CCSN in rapidly rotating massive stars. Simulations of CCSN indicate several methods for GW emission at frequencies of several hundred Hz to 1 kHz, but the amplitude of the emission is highly uncertain [48]. The most optimistic emission models

arise from the pulsations of a proto-neutron star core, which may release $10^{-7} M_\odot c^2$ in GWs in a narrow frequency band around 1 kHz [49,50].

Both types of GRBs are expected to result in a compact object (a neutron star or black hole) with an accretion disk. Instabilities in the accretion disk can emit significant energy in GWs. Various semianalytical scenarios have been proposed which release up to $10^{-2} M_\odot c^2$–$10^{-1} M_\odot c^2$ in GWs, all of which correspond to the development of rotational instabilities in the accretion disk or central engine. Bar mode instabilities, in the $l = 2$, $m = 2$ non-axisymmetric mode, are optimistic models for GW emission in CCSN; typical frequencies are between 500 Hz and 2 kHz [51,52]. If the deformation remains coherent for $\sim$100 ms, $E_{\mathrm{GW}} \sim 0.1 M_\odot c^2$ could be emitted at 1 kHz. An accretion disk that cools rapidly enough to become self-gravitating may fragment into one or more smaller bodies and generate an inspiral-like signal that persists to higher frequencies [53]. The infall of matter from a rapidly-rotating accretion disk could generate nonaxisymmetric instabilities in a neutron star and produce GWs in the $\sim$700 Hz–2.14 kHz band for many seconds following the merger [54]. Instead of an accretion disk, a torus may form around the black hole and convert the spin energy of the black hole into GWs in the 1 kHz–2 kHz band [55,56]. Numerical simulations have produced similar signals [36,57].

Finally, the oscillation of quasinormal modes of a hypermassive neutron star or perturbed black hole can emit GWs with large amplitudes [58–60], although the peak emission is typically outside the search band used in this analysis.

III. GW OBSERVATORIES

The GEO 600 detector (G1), located near Hannover, Germany, is a dual-recycled Michelson interferometer with single-folded arms 600 m in length [61,62]. GEO 600 implements a number of advanced interferometric techniques such as signal recycling and squeezed light to improve sensitivity at frequencies above a few hundred Hz [63,64]. The LIGO [65] and Virgo [66] observatories are power-recycled interferometers of similar design, with Fabry-Perot cavities in the arms to increase the effective arm length and improve the sensitivity to GWs. There are two LIGO observatories, located in Hanford, WA, USA and Livingston, LA, USA [65]. The Hanford site housed two interferometers, one with 4 km long arms, which is referred to as H1, and another with 2 km long arms which is referred to as H2. The H2 instrument ceased data-taking operations in July 2009. The Livingston observatory has a single interferometer with 4 km long arms, referred to as L1. The Virgo detector, known as V1, has 3 km long arms and is located in Cascina, Italy [66].

The GEO 600 detector has been operated with high duty cycle since 2006, with occasional short breaks for invasive
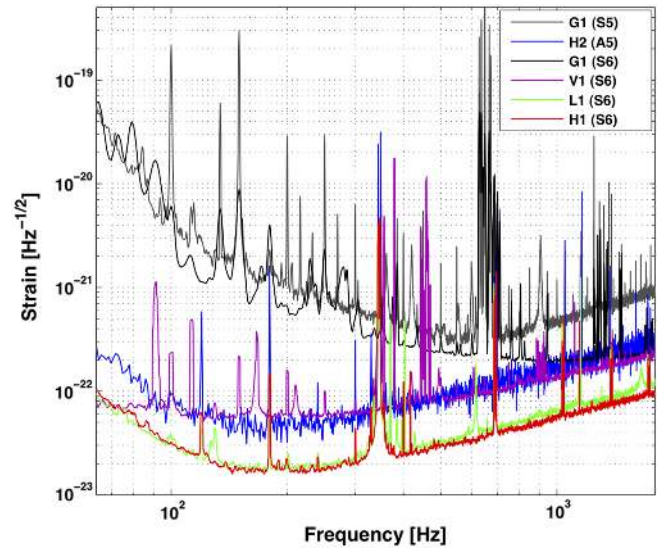
FIG. 1 (color online). Strain sensitivity for the detectors used in this analysis. GEO 600 is shown at two epochs from the S5 and S6 science runs.

configuration changes and instrumental upgrades. The LIGO and Virgo observatories have taken data in a series of science runs, during which the detector is kept in its most sensitive state, separated by periods of intense commissioning activity.

The fifth LIGO science run (S5) started on November 1, 2005 and ended on October 1, 2007. During S5, the H1, H2, and L1 interferometers operated near their design sensitivity, with duty cycles of approximately 70%. The H2 interferometer continued to collect science data on an opportunistic basis from October 1, 2007 to June 1, 2009, during a period of instrumental upgrades to the H1 and L1 detectors. The sixth LIGO science run (S6) was held from July 7, 2009 to October 20, 2010. In S6, the H1 and L1 were operated with duty cycles of 52% and 47%, respectively, and both surpassed their sensitivities from S5.

The first Virgo science run (VSR1) started on May 18, 2007 and ended on October 1, 2007. The second Virgo science run (VSR2) was held from July 7, 2009 to January 8, 2010, and the third Virgo science run (VSR3) was held from August 11, 2010 to October 19, 2010. The fourth Virgo science run (VSR4) was held from May 20, 2011 to September 5, 2011, followed by a period of opportunistic data collection that ended on November 3, 2011. Virgo's duty cycle was 71% for VSR2-4.

Figure 1 shows representative sensitivity curves, in terms of amplitude spectral density, of the GEO 600, LIGO, and Virgo interferometers during these science runs.

IV. SEARCH METHODS

The coherent analysis algorithm used in this search is X-PIPELINE [67], and the overall search procedure follows that used in previous searches for generic GW signals

during the S5-VSR1 [26] and S6-VSR2,3 [27] science runs.[1] Following the method of the S6-VSR2,3 search, we employ a circularly polarized GW signal model; this is motivated by our expectation that the rotation axis of the GRB central engine is likely pointed at the observer, to within $\sim 10°$. In this section we give a brief description of the analysis pipeline and introduce new techniques to accommodate the high frequency sensitivity of the GEO 600 detector and the sky localization uncertainties of the *Fermi* GBM [68].

A. Analysis procedure

Data from GW detectors surrounding the time of a GRB are divided into an *off-source window*, which is used to characterize the background of transient signals around the time of the GRB, and an *on-source window*, which is searched for GW signals. To allow for possible GW precursors from, for example, the CCSN associated with long GRBs, the on-source window is [−600, +60] s around the onset time of the GRB event. For very long-lasting GRBs, the on-source window is extended to include the entire T_{90} time of the event, defined as the time interval over which 90% of the total background-subtracted photon counts are observed. The standard off-source window is ± 1.5 hours around the time of the GRB trigger, excluding the on-source window.

In the analysis, the time-series data from each detector are whitened using linear predictor error filters; this removes periodic signals (for example from mechanical resonances in the detector) which are present over long time scales. The detector data streams are time-shifted to synchronize the arrival time of a GW signal incident from the sky position of the GRB. Discrete Fourier transforms are performed for various time resolutions, ranging from $1/4$ s to $1/256$ s, to maximize the search sensitivity to GW bursts of different duration. For each detector data stream, and each resolution, the time-frequency maps generated by the discrete fourier transform are weighted by the sensitivity of the detector to the *plus* and *cross* polarizations of GWs incident from the GRB sky location. X-PIPELINE then constructs linear combinations of the time-frequency maps of the detector data, and a clustering algorithm is used to search for groups of loud pixels in the combined map. For clusters with significant excess energy, the signal strength in the *N*-dimensional space of detector data streams is projected along directions that are parallel and perpendicular to the projection of a true GW signal from the GRB sky location. A cluster whose signal energy lies in a direction orthogonal to a true GW signal (for example, with

larger amplitude in the least sensitive detector) is rejected by the analysis; these *coherent consistency checks* are described in detail in [67,69]. Clusters (now referred to as events) that survive the consistency checks are ranked by their likelihood to be a circularly polarized GW signal, measured using a Bayesian detection statistic described in [69,70]. Before considering the events found in the on-source region, the off-source results are examined for data quality issues and sensitivity to simulated GW waveforms.

To estimate the rate of background events, the analysis of the off-source data is repeated many hundreds of times, with unphysical *time slides* of > 3 s applied to the time series from one of the detectors. This technique robustly estimates the frequency at which random noise fluctuations in the detectors may appear to be a true GW signal with large amplitude in the on-source window. A typical search with X-PIPELINE will perform $\mathcal{O}(10^3)$ time slides on the data in the off-source window, enough to quantify the rate of background events to a *false-alarm rate* (FAR) below 10^{-6} Hz. Repeating the analysis for hundreds of time slides is the most computationally intensive portion of the search.

To determine if a GW is present in the data, the loudest on-source event is compared to the distribution of off-source events. The *false-alarm probability* (FAP), or *p-value* of this event is defined as the fraction of off-source events with equal or greater significance; this is an empirical measure of the probability of obtaining such an event in the on-source, under the null hypothesis. Events with $p < 0.01$ are followed up with detailed investigations to determine if the events can be associated with non-GW noise artefacts in the detectors.

B. Sky location uncertainty

The sky localizations of GRBs detected by the *Fermi* GBM can have uncertainty regions covering hundreds of square degrees, depending on the gamma-ray flux and energy spectrum [71]. In a coherent search for GWs associated with GRBs, performing the analysis using an incorrect sky location can reduce the significance of a GW signal in two ways.

First, the analysis will incorrectly estimate the sensitivity of each detector to GWs from the sky location of the GRB. This can result in loss of coherent signal energy when the time-frequency maps from each detector are combined. Over most of the sky, the antenna factors for GW observatories change slowly as a function of sky location, usually a few percent over a few degrees. We have performed empirical tests of the robustness of our coherent detection statistic to variations in sky localization of several degrees, and for the majority of positions on the sky the loss of signal is of order a few percent. We conclude that this effect is not large enough to alter the results of our search.

Second, and more significantly, an error in the sky location will lead to an erroneous time shift of the detector data vectors when synchronizing the arrival time of a GW

---

[1]The most recent searches for short-duration GWs associated with GRBs have included a modeled search for CBC signals (either NS-NS or NS-BH) on the short GRBs included in the sample [27,32]. Due to the sensitivity of the GEO 600 detector at low frequencies (where most of the power of a CBC waveform is emitted) we did not perform a dedicated search for CBCs as part of our analysis.

signal across detectors. For pairs of ground-based detectors the difference in arrival times is $\mathcal{O}(10)$ milliseconds, and an error in the sky location of a few degrees could introduce incorrect synchronizations of a millisecond or more. This results in the misalignment of a GW signal by several periods for waveforms with frequency content above 1 kHz, and when the data vectors are combined the coherent signal energy will be diminished. In the worst case, the waveform will be shifted by a half-period between the detectors, and the signal will cancel entirely in the coherent summation.

The standard solution in coherent GW searches is to repeat the analysis over a discrete grid of sky positions covering most of the uncertainty region. The grid step is chosen so that the timing synchronization error between any position in the sky localization error box and the nearest analysis grid point is less than 25% of the period for the highest-frequency GW signals included in the search. For simplicity, the step size is held constant across the search area; for uncertainty regions with radii of $\mathcal{O}(10)$ degrees the variation in the magnitude of the time-of-arrival correction does not change enough to warrant a variable grid spacing.

Previous searches have used regular grids of concentric circles around the best estimate of the source location, covering at least 95% of the sky location probability distribution. For the *Fermi* GBM, the 68% containment radius is typically 2°–3° due to statistical effects, and the localizations have additional systematic errors of several degrees. As a result, the 95% containment region can cover hundreds of square degrees, and a search for GW signals with frequencies larger than a few hundred Hz would require tiling the search area with many hundreds of search points. At each grid point the coherent signal combination will have to be recomputed using the new time-of-arrival corrections. The background estimation for a search grid of this size will typically require $\mathcal{O}(10^4)$ CPU hours, depending on the size of the GRB uncertainty region, the sky location, and the GW detectors included in the search. Even on computing clusters with thousands of CPU cores,[2] the analysis for a single GBM event can take several hours to several days to complete.

Our solution is to cover the search region with a linear grid, arranged parallel to the maximum gradient of change in the relative time-of-arrival between detectors. In the case of a 2-detector network, we find that such a pattern is sufficient to capture the dominant source of coherent energy variability as the likelihood is calculated across the GRB uncertainty region. A comparison of the circular and linear search grids for the *Fermi* event GRB 080906B is shown in Fig. 2.
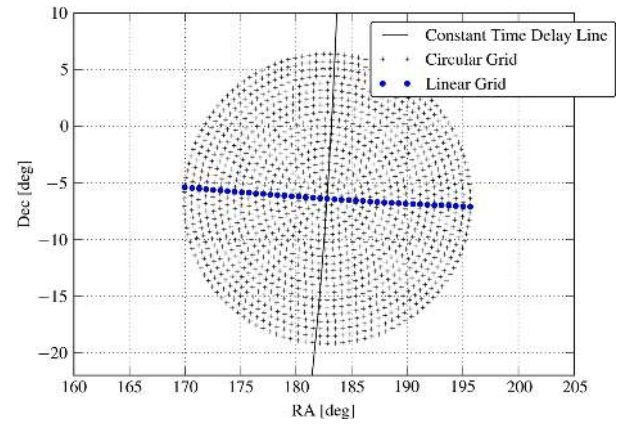

FIG. 2 (color online). Example linear (blue circles) and circular (black crosses) grids for a search for GW signals up to 1792 Hz. The localization for the *Fermi* GBM event GRB 080906B is shown. The linear search grid contains 41 sky positions, arranged in the direction of the gradient of the time shift been the H2 and G1 detectors. The circular grid contains 1324 sky positions and would require several days to analyze on a massively parallel computing cluster. Both search grids cover the 95% containment region for the GBM sky location probability distribution. The GBM statistical error for this event is 1.6°.

For two detectors separated by a distance d, the difference in time of arrival for a GW is

$$t = \frac{d \cos \theta}{c} \qquad (1)$$

where θ is the angle between the interdetector baseline and the line-of-sight to the GRB, and c is the speed of light. For a maximum time-delay error tolerance of $dt \leq \alpha$, the corresponding spacing $d\theta$ between grid points is

$$|d\theta| \leq \frac{2c}{d \sin \theta} \alpha. \qquad (2)$$

For our search band of 64 Hz–1792 Hz,[3] we choose $\alpha = 0.14$ ms, equal to 25% of a cycle at 1792 Hz. The extent of the linear grid is determined by the 95% containment radius for the given GRB localization. For events localized by the *Swift* BAT [72], we use a search grid of a single point. For events localized by the *Fermi* GBM [68], we use $1.65\sigma_{\text{stat+sys}}$, where σ_{stat} is the GBM statistical error for the GRB (typically 2°–3°), and σ_{sys} is a 7.5° systematic error [73–75]. The $1.65\sigma_{\text{stat+sys}}$ uncertainty radius corresponds to 95% containment for a von Mises-Fisher distribution on a sphere [71].

---

[3]The low frequency limit was chosen to match previous analyses for which the data conditioning has been well tested. The high-frequency limit is the Nyquist frequency of the detector data (2048 Hz) minus the widest frequency resolution used in the search (256 Hz).

For a handful of GRBs, direct comparisons were made between the linear grid and the full circular tiling, by calculating the sensitivity of the search to simulated GW signals with sky positions distributed across the 95% containment region. The results for the two methods were nearly identical. Using the linear grid, the signal amplitudes required for detection were within a few percent of those obtained by the same analysis using the circular grid. Furthermore, the analysis using the linear grid was completed in a fraction of the time required for the circular grid, and typically required $\mathcal{O}(10^3)$ or fewer CPU hours, depending on the detectors used in the analysis. Using computing clusters with thousands of CPU cores, it was possible to analyze some GRBs localized by the GBM in less than three hours.

C. Sky localization using the linear grid

One of the primary goals of GW searches is the prompt localization of the source sky location, for follow-ups by EM astronomers. Currently, very few GRBs detected by the *Fermi* GBM are examined for optical counterparts, due to the resources necessary to search an uncertainty region of hundreds of square degrees. The detection of a GW signal associated with a GRB will be of tremendous interest to the astronomical community, and any improvement of the GBM localization will increase the chances that astronomers could detect an optical, radio, or X-ray counterpart to the gamma-ray and GW signal.

If a GW signal is detected in the on-source window, X-PIPELINE can localize the source to within a few degrees along the axis of the linear grid, depending on the frequency content of the signal and its duration; this is illustrated in Fig. 3. The sky location of the event is chosen as the point on the search grid that maximizes the coherent energy in the detected GW signal. For a search using data from two widely-separated detectors, the localization from the GW signal is limited to an annulus on the sky, encircling the line connecting the two detectors [76]; in principle, this localization cannot be improved upon in the direction perpendicular to the search grid. For searches using data from three or more widely-separated detectors, a GW signal can be localized in both dimensions, and in this case the computational cost of the full circular tiling may be worthwhile for event follow-ups. Efforts to characterize X-PIPELINE's ability to localize signals using three or more detectors are ongoing.

As a demonstration of the localization accuracy, the observed errors for 600 simulated short-duration GW signals with central frequencies of 150 Hz and 1.5 kHz are shown in a cumulative histogram in Fig. 4. The localization of the high-frequency signals is superior to that of the low-frequency signals due to the greater phase sensitivity to variations in sky position. For signals at 1.5 kHz, 95% of the simulations were reconstructed to less than 2.5° along the axis of the linear grid; this provides
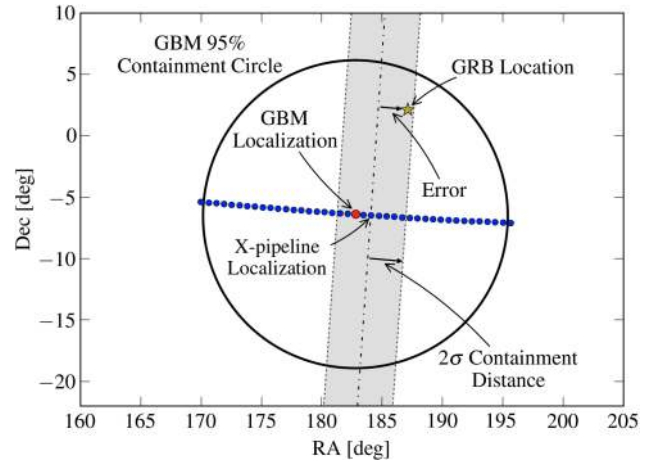

FIG. 3 (color online). Sky localization using the linear search grid. The X-PIPELINE analysis will localize a detected GW signal to the point on the linear grid closest to the true injected signal, within errors due to noise fluctuations. The containment distance is a function of the frequency and duration of the GW signal, and can be empirically measured for each GRB as part of the GW analysis pipeline; no additional processing time is required. In this example, the 2σ containment distance is about 2.5°. The coordinates of the shaded region can be disseminated to electromagnetic (EM) astronomers for follow-up by wide-field telescopes.
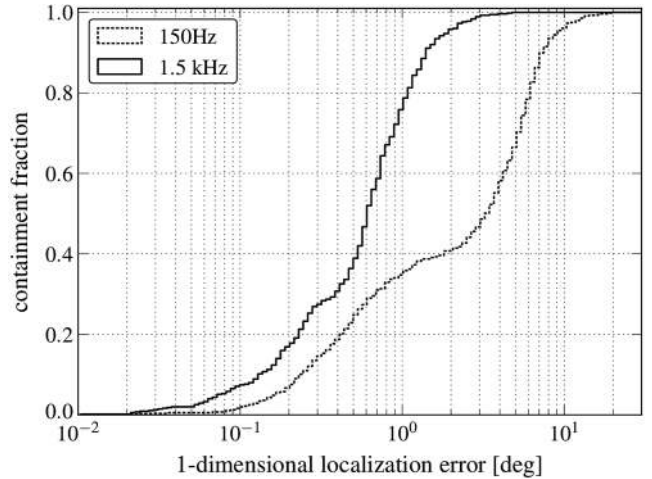
FIG. 4. Errors in sky localization reconstruction, for a simulated GBM event in real GW detector data with the H1-V1 detector network. For each frequency, six hundred sine-Gaussian waveforms with quality factor $Q = 9$ were analyzed using a linear grid covering a 16.5° uncertainty region with 59 grid points. The sky location of each simulation was jittered following a Fisher distribution with $\sigma = 10°$, and the amplitude was chosen to correspond to the 90% detection threshold. The one-dimensional error in the reconstructed location was measured along the axis of the search grid. High-frequency waveforms provide greater sensitivity to the time-of-arrival correction across the search grid.

an empirical measurement of the 2σ uncertainty in X-PIPELINE's localization.

V. GRB SAMPLE AND SEARCH RESULTS

We have applied this technique in a search for GW signals associated with GRBs, using data from the GEO 600, LIGO, and Virgo observatories. The GRB events were obtained from the gamma-ray burst coordinates network (GCN) [77], supplemented by the *Swift* and *Fermi* on-line catalogues,[4] as well as the published *Fermi* four-year catalogue [78]. Most of the GRBs in our sample were detected by *Swift* and *Fermi*; a few of the GRBs were detected by other space borne experiments such as *INTEGRAL* [79], *AGILE* [80], or *MAXI* [81].

We analyze GRBs which were observed when GEO 600 plus one other observatory was taking science-quality data. For the LIGO and Virgo interferometers, "science-mode" is a rigorous definition, and identifies times when the detector configuration is stable and the interferometer is operating in a resonant, low-noise state. Unbroken intervals of "science mode" operation are referred to as "science segments"; these may last from several minutes to many hours, depending on the environmental conditions and the schedule of instrument upgrades. Incremental configuration changes are sometimes made in the periods between science segments. GEO 600 has no strictly-defined "science mode," and collects data on an opportunistic basis between commissioning activities. In this so-called "Astrowatch" operation, efforts are made to collect as much calibrated data as possible given the constraints of commissioning and improvements to the detector.

In our search, no distinction is made between short GRBs and long GRBs, and the analysis is performed without regard to the observed GRB fluence or redshift (if known). Data segments from GW detectors which are flagged as being of poor quality are excluded from the analysis, and GRBs for which there is insufficient data surrounding the GRB event time are not analyzed. We discard the analysis results of GRBs that are determined to have exceptionally high rates of background events or exceptionally poor sensitivity to GWs from the sky location of the GRB; this can result from, for example, sources of environmental or instrumental noise at the time of the GRB [82–86], or a GRB sky location that includes one of the sensitivity null points of the detectors. Finally, the sensitivity of the GEO 600 detector can change by 20% or more at frequencies > 1 kHz, depending on whether or not squeezed light states are being injected. A change in sensitivity of this magnitude may bias the background estimation if it occurs partway through the off-source window around a GRB. In this analysis, no GRB off-source (or on-source) windows include times when GEO 600 changed from a squeezing to nonsqueezing state, or vice versa.

In the epoch considered for our search (Feb 4, 2006 to Nov 3, 2011), there were 152 GRBs with sufficient science data to analyze. For 130 GRBs the results of the background estimation demonstrated good sensitivity to potential GW signals, and for each of these GRBs we calculate the p-value for the loudest event in the on-source. Three GRBs in our sample had on-source events with $p < 0.01$:

(i) GRB 060502A, a *Swift* BAT detection with $T_{90} = 28.4$ s and an observed redshift of $z = 1.51$ [87], was analyzed using data from the L1 and G1 detectors. There were three significant events in the on-source window. An examination of the data quality around the time of the GRB revealed non-stationary noise in the L1 detector, associated with increased ground motion due to a magnitude 5.0 earthquake in Costa Rica. All three on-source events occurred during a segment of time that was identified as likely to experience an increased rate of transient signals, due to larger than normal seismic vibrations. Since 35% of the on-source window for this GRB was flagged as having elevated ground motion, we veto the three events and do not include this GRB in the cumulative results.

(ii) GRB 080816A, a *Fermi* GBM detection with $T_{90} = 4.6$ s, was analyzed using data from the H2
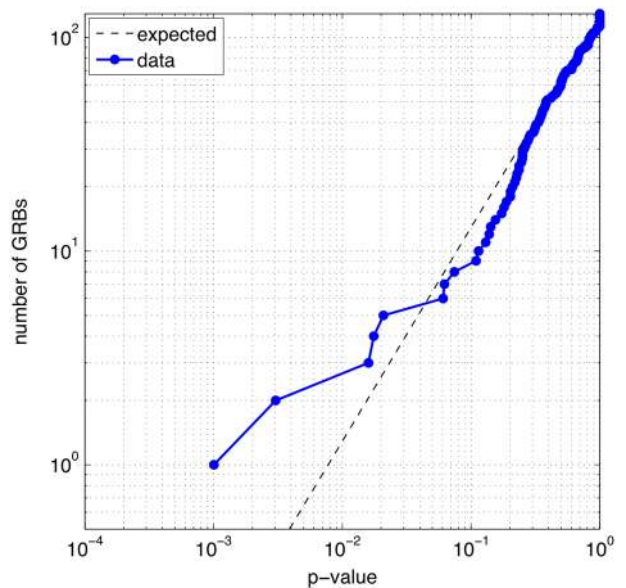

FIG. 5 (color online). Cumulative p-value distribution from the analysis of 129 GRBs. The dashed line gives the expected distribution under the null hypothesis. The most significant on-source event, with $p = 0.001$, is associated with GRB 080816A; a study of detector data at the time of the event yields potential instrumental causes for the signal in the GW channel. The probability that our cumulative distribution is due to background is 19.3%, which indicates that the data is consistent with no subthreshold GW events being present.

---

[4]http://heasarc.gsfc.nasa.gov/W3Browse/fermi/fermigbrst.html, http://swift.gsfc.nasa.gov/archive/grb_table

TABLE I. Information and limits on associated GW emission for each of the analyzed GRBs. The first four columns are: the GRB name in YYMMDD format; the trigger time; and the sky position used for the GW search (right ascension and declination). The fifth column gives the GW detector network used in the analysis. Columns six and seven display the upper limits from each GRB: the 90% confidence upper limits on the strain amplitude for circularly polarized 500 Hz and 1 kHz sine-Gaussian waveforms, in units of 10^{-21} Hz$^{-1/2}$. The last column gives the γ-ray detector that provided the event time, sky location, sky position uncertainty, and T_{90} used for the search (*Swift* BAT, *Fermi* GBM, *INTEGRAL* IBIS, *SuperAGILE*, or *MAXI*). For three GRBs marked with a †, narrowband nonstationary noise in the GEO 600 detector at frequencies above 1 kHz may have reduced our sensitivity to GW signals.

GRB name	UTC Time	RA	Dec.	Network	90% ULs ($\times 10^{-21}$ Hz$^{-1/2}$) 500 Hz	1 kHz	γ-Ray Detector
060424	04:16:19	$0^h29^m26^s$	$36°47'$	G1L1	1.46	3.01	BAT
060512	23:13:20	$13^h02^m58^s$	$41°13'$	G1L1	1.48	2.53	BAT
060522	02:11:18	$21^h31^m49^s$	$2°53'$	G1L1	1.93	2.35	BAT
060602A	21:32:12	$9^h58^m19^s$	$0°18'$	G1L1	2.55	4.39	BAT
060604	18:19:00	$22^h28^m54^s$	$-10°56'$	G1L1	1.37	2.58	BAT
060708	12:15:59	$0^h31^m17^s$	$-33°45'$	G1L1	1.61	2.88	BAT
060801	12:16:15	$14^h11^m56^s$	$16°59'$	G1L1	3.95	3.37	BAT
060929	19:55:01	$17^h32^m35^s$	$29°50'$	H2G1	2.22	4.93	BAT
061110B†	21:58:45	$21^h35^m38^s$	$6°52'$	G1L1	2.91	7.42	BAT
070328	03:53:53	$4^h20^m27^s$	$-34°04'$	G1L1	1.42	2.21	BAT
070406	00:50:38	$13^h15^m52^s$	$16°28'$	G1L1	1.37	2.31	BAT
070509	02:48:27	$15^h51^m35^s$	$-78°39'$	G1L1	1.49	2.13	BAT
070517	11:20:58	$18^h30^m14^s$	$-62°18'$	H2G1	2.60	4.12	BAT
070925	15:52:32	$16^h52^m52^s$	$-22°02'$	G1V1	3.01	3.98	IBIS
080207†	21:30:21	$13^h50^m03^s$	$7°29'$	G1V1	4.09	11.1	BAT
080229A	17:04:59	$15^h12^m52^s$	$-14°41'$	H2G1	2.21	4.10	BAT
080303†	09:10:35	$7^h28^m11^s$	$-70°13'$	H2G1	3.07	7.78	BAT
080319A	05:45:42	$13^h45^m22^s$	$44°04'$	H2G1	2.07	4.02	BAT
080319B	06:12:49	$14^h31^m40^s$	$36°17'$	H2G1	2.17	3.13	BAT
080319C	12:25:56	$17^h16^m01^s$	$55°23'$	H2G1	NaN	3.09	BAT
080328	08:03:04	$5^h21^m58^s$	$47°31'$	H2G1	2.63	4.28	BAT
080330	03:41:16	$11^h17^m05^s$	$30°36'$	G1V1	5.72	30.6	BAT
080405	09:18:55	$10^h50^m23^s$	$-4°15'$	H2G1	1.95	3.07	BAT
080411	21:15:32	$2^h31^m50^s$	$-71°17'$	H2G1	2.07	3.15	BAT
080514B	09:55:56	$21^h31^m16^s$	$0°44'$	H2G1	3.02	15.8	AGILE
080515	06:01:13	$0^h12^m36^s$	$32°34'$	H2G1	3.16	5.38	BAT
080524	04:13:00	$17^h54^m04^s$	$80°08'$	H2G1	2.03	2.81	BAT
080603A	11:18:15	$18^h37^m37^s$	$62°44'$	H2G1	2.38	3.14	IBIS
080702A	11:50:43	$20^h52^m14^s$	$72°16'$	H2G1	3.18	4.18	BAT
080703	19:00:13	$6^h47^m16^s$	$-63°12'$	H2G1	2.53	3.77	BAT
080717A	13:02:35	$9^h49^m12^s$	$-70°00'$	H2G1	1.78	2.98	GBM
080816A	12:04:18	$10^h24^m48^s$	$42°36'$	H2G1	3.01	4.97	GBM
080830A	08:50:16	$10^h40^m23^s$	$30°48'$	H2G1	4.34	25.9	GBM
080905A	11:58:55	$19^h10^m40^s$	$-18°51'$	H2G1	2.26	4.73	BAT
080905C	13:41:29	$6^h27^m35^s$	$-69°48'$	H2G1	2.99	5.04	GBM
080906B	05:05:11	$12^h11^m12^s$	$-6°24'$	H2G1	4.20	10.6	GBM
080916A	09:45:21	$22^h25^m08^s$	$-57°01'$	H2G1	2.73	3.93	BAT
081003A	13:46:12	$17^h29^m30^s$	$16°33'$	H2G1	2.81	4.22	IBIS
081007	05:23:52	$22^h39^m50^s$	$-40°08'$	H2G1	3.76	6.22	BAT
081009A	03:20:58	$16^h41^m59^s$	$18°23'$	H2G1	2.58	4.11	GBM
081016A	06:51:31	$17^h02^m17^s$	$-23°19'$	H2G1	2.77	6.22	IBIS
081017B	11:22:37	$7^h15^m59^s$	$-15°12'$	H2G1	3.03	4.30	GBM
081021A	09:33:28	$12^h41^m12^s$	$-25°36'$	H2G1	2.59	3.43	GBM
081028B	12:55:08	$1^h03^m59^s$	$-27°12'$	H2G1	2.52	3.71	GBM
081101	11:46:32	$6^h23^m20^s$	$-0°06'$	H2G1	2.02	3.15	BAT
081115A	21:22:28	$12^h42^m23^s$	$63°17'$	H2G1	17.0	8.23	GBM
081119A	04:25:27	$23^h6^m00^s$	$30°00'$	H2G1	2.92	3.88	GBM
081129A	03:52:04	$4^h12^m48^s$	$-54°54'$	H2G1	3.23	5.22	GBM
081203A	13:57:11	$15^h32^m17^s$	$63°30'$	H2G1	2.05	2.91	BAT

(Table continued)

TABLE I. (*Continued*)

GRB name	UTC Time	RA	Dec.	Network	90% ULs (×10^{-21} Hz$^{-1/2}$) 500 Hz	1 kHz	γ-Ray Detector
081203B	13:51:59	15^{h}15^{m}09^s	44°25′	H2G1	2.26	3.86	BAT
081204B	12:24:25	10^{h}03^{m}12^s	30°30′	H2G1	5.81	7.15	GBM
081206C	23:41:50	3^{h}37^{m}11^s	−8°36′	H2G1	7.47	NaN	GBM
081224A	21:17:55	13^{h}26^{m}47^s	75°05′	H2G1	3.53	4.37	GBM
081228	01:17:40	2^{h}37^{m}54^s	30°50′	H2G1	2.55	4.23	BAT
090123	07:51:56	0^{h}27^{m}10^s	−23°30′	H2G1	2.90	6.70	BAT
090201	17:47:02	6^{h}08^{m}12^s	−46°36′	H2G1	3.50	3.11	BAT
090213A	05:39:25	22^{h}02^{m}24^s	−55°00′	H2G1	2.03	3.02	GBM
090222A	04:17:09	7^{h}54^{m}23^s	45°00′	H2G1	2.59	3.90	GBM
090305A	05:19:51	16^{h}07^{m}03^s	−31°34′	H2G1	3.44	5.02	BAT
090306C	05:52:05	9^{h}07^{m}59^s	57°00′	H2G1	2.63	3.35	GBM
090307A	03:46:37	16^{h}19^{m}55^s	−28°38′	H2G1	2.12	2.93	BAT
090307B	03:59:57	11^{h}30^{m}48^s	−23°54′	H2G1	8.70	NaN	GBM
090413A	02:55:57	17^{h}45^{m}59^s	−9°12′	H2G1	2.43	3.17	GBM
090417A	13:17:23	2^{h}19^{m}58^s	−7°08′	H2G1	3.08	5.37	BAT
090418B	09:00:21	15^{h}03^{m}38^s	17°13′	H2G1	3.01	4.00	BAT
090712A	03:51:05	4^{h}40^{m}22^s	22°31′	G1V1	2.21	3.31	BAT
090713A	00:29:28	18^{h}59^{m}11^s	−3°19′	G1V1	2.85	3.41	GBM
090715B	21:03:15	16^{h}45^{m}21^s	44°50′	G1V1	1.59	1.64	BAT
090718B	18:17:43	18^{h}16^{m}24^s	−36°23′	G1H1	0.85	1.58	GBM
090804A	22:33:20	8^{h}41^{m}36^s	−11°18′	G1V1	1.43	1.95	GBM
090807B	19:57:59	21^{h}47^{m}35^s	7°13′	G1V1	2.94	5.34	GBM
090810A	18:44:44	7^{h}45^{m}43^s	−17°28′	G1V1	2.19	3.99	GBM
100131A	17:30:58	8^{h}01^{m}36^s	16°23′	L1G1	3.18	7.57	GBM
100331A	00:30:22	17^{h}24^{m}14^s	−58°56′	L1G1	2.39	2.58	IBIS
100417A	03:59:44	17^{h}25^{m}12^s	50°23′	G1L1	26.7	7.05	GBM
100510A	19:27:07	23^{h}43^{m}12^s	−35°36′	L1G1	2.91	3.76	MAXI
100511A	00:49:56	7^{h}17^{m}12^s	−4°39′	L1G1	5.66	8.70	GBM
100528A	01:48:01	20^{h}44^{m}24^s	27°48′	L1G1	2.20	2.43	AGILE
100625A	18:32:28	1^{h}03^{m}11^s	−39°05′	L1G1	2.56	3.90	BAT
100703A	17:43:37	0^{h}38^{m}05^s	−25°42′	L1G1	3.13	3.89	IBIS
100704A	03:35:08	8^{h}54^{m}33^s	−24°12′	H1G1	2.60	3.73	BAT
100719C	19:48:08	15^{h}25^{m}38^s	18°33′	H1G1	65.3	17.0	GBM
100805A	04:12:42	19^{h}59^{m}23^s	52°37′	L1G1	2.23	2.39	BAT
100807A	09:13:13	3^{h}41^{m}07^s	67°39′	L1G1	2.04	1.60	BAT
100814B	08:25:26	8^{h}11^{m}16^s	18°29′	L1G1	3.63	10.0	GBM
100901A	13:34:10	1^{h}49^{m}00^s	22°45′	G1V1	7.36	6.16	BAT
100906A	13:49:27	1^{h}54^{m}47^s	55°38′	H1G1	1.16	1.16	BAT
100907A	18:01:12	11^{h}49^{m}09^s	−40°37′	G1V1	6.40	6.15	GBM
100915B	05:49:38	5^{h}41^{m}34^s	25°05′	L1G1	2.59	3.18	IBIS
101008A	16:43:15	21^{h}55^{m}31^s	37°03′	G1V1	4.16	2.79	BAT
101017B	14:51:29	1^{h}49^{m}52^s	−26°33′	G1V1	4.37	3.37	GBM
110604A	14:49:46	18^{h}04^{m}00^s	18°28′	G1V1	4.70	3.18	BAT
110605A	04:23:32	0^{h}59^{m}47^s	52°27′	G1V1	1.82	1.49	GBM
110610A	15:21:32	20^{h}32^{m}49^s	74°49′	G1V1	2.12	1.93	BAT
110616A	15:33:25	18^{h}17^{m}48^s	−34°01′	G1V1	2.17	1.60	GBM
110618A	08:47:36	11^{h}47^{m}13^s	−71°41′	G1V1	2.11	1.61	GBM
110624A	21:44:26	4^{h}20^{m}04^s	−15°57′	G1V1	2.12	1.79	GBM
110625A	21:08:28	19^{h}07^{m}00^s	6°45′	G1V1	2.96	2.15	BAT
110626A	10:44:54	8^{h}47^{m}38^s	5°33′	G1V1	3.24	2.32	GBM
110629A	04:09:58	4^{h}37^{m}28^s	25°00′	G1V1	3.09	2.86	GBM
110702A	04:29:29	0^{h}22^{m}28^s	−37°39′	G1V1	5.70	6.70	GBM
110706A	04:51:04	6^{h}40^{m}19^s	6°08′	G1V1	5.94	5.64	GBM
110709A	15:24:29	15^{h}55^{m}34^s	40°55′	G1V1	2.60	2.07	BAT
110709B	21:32:39	10^{h}58^{m}40^s	−23°28′	G1V1	3.96	3.18	BAT

(*Table continued*)

TABLE I. (*Continued*)

GRB name	UTC Time	RA	Dec.	Network	90% ULs ($\times 10^{-21}$ Hz$^{-1/2}$) 500 Hz	1 kHz	γ-Ray Detector
110709C	11:06:53	$10^h21^m31^s$	$23°07'$	G1V1	2.59	2.02	GBM
110709D	20:40:50	$10^h24^m50^s$	$-41°47'$	G1V1	3.07	2.87	GBM
110710A	22:53:51	$15^h16^m21^s$	$48°23'$	G1V1	1.92	1.61	GBM
110716A	00:25:20	$21^h58^m43^s$	$-76°58'$	G1V1	2.86	2.48	GBM
110722A	16:39:17	$14^h20^m14^s$	$5°00'$	G1V1	2.76	2.03	GBM
110729A	03:25:06	$23^h33^m33^s$	$4°58'$	G1V1	2.04	1.64	GBM
110730B	15:50:44	$22^h20^m24^s$	$-2°53'$	G1V1	2.86	2.19	GBM
110731A	11:09:30	$18^h42^m03^s$	$-28°32'$	G1V1	1.98	1.51	BAT
110801A	19:49:42	$5^h57^m39^s$	$80°57'$	G1V1	2.17	1.99	BAT
110803A	18:47:25	$20^h01^m40^s$	$-11°26'$	G1V1	6.02	4.13	GBM
110809A	11:03:34	$11^h28^m40^s$	$-13°55'$	G1V1	3.91	3.48	GBM
110817A	04:35:12	$22^h24^m09^s$	$-45°50'$	G1V1	3.47	2.77	GBM
110818A	20:37:49	$21^h09^m29^s$	$-63°58'$	G1V1	3.55	3.01	BAT
110825B	06:22:11	$16^h45^m14^s$	$-80°16'$	G1V1	2.35	2.14	GBM
110827A	00:01:52	$10^h56^m14^s$	$53°49'$	G1V1	4.11	3.41	BAT
110828A	13:48:15	$7^h22^m19^s$	$-23°48'$	G1V1	4.45	4.91	GBM
110831A	06:45:27	$23^h29^m24^s$	$33°39'$	G1V1	5.34	3.70	GBM
110903A	02:39:55	$13^h08^m14^s$	$58°59'$	G1V1	3.02	2.96	BAT
110903B	00:13:06	$10^h56^m50^s$	$42°04'$	G1V1	18.8	5.62	GBM
110904A	02:58:16	$23^h58^m45^s$	$35°53'$	G1V1	1.86	1.53	GBM
110904C	12:44:19	$21^h34^m57^s$	$23°56'$	G1V1	14.3	8.70	GBM
111008B	23:49:01	$14^h43^m00^s$	$-5°40'$	G1V1	3.35	4.31	GBM
111022A	16:07:04	$18^h23^m29^s$	$-23°40'$	G1V1	3.88	3.03	BAT
111022B	17:13:04	$7^h15^m42^s$	$49°39'$	G1V1	4.29	3.14	BAT
111103C	22:45:06	$13^h26^m19^s$	$-43°09'$	G1V1	1.58	1.59	GBM

and G1 detectors. There was one significant on-source event, with $p = 0.001$. A signal processing algorithm revealed multiple instrumental channels in the H2 detector with nonstationary noise at the time of the event. The nature of the instrumental noise is not understood, but the signal in the GW channel is unlikely to be of astrophysical origin. No redshift observations are available for this GRB.

(iii) GRB 090712A, a *Swift* BAT detection with $T_{90} = 145$ s, was analyzed using data from the G1 and V1 detectors. There was one significant on-source event, with $p = 0.003$. While we find no plausible instrumental or environmental cause for the event, the observed p-value for this GRB is not significant in a data set containing 129 GRBs. No redshift observations are available for this GRB.

The distribution of p-values for the most significant event found in the on-source window for each of the 129 GRBs is shown in Fig. 5. To test the sample of GRBs for a population of subthreshold GW signals, we use a weighted binomial test to check that the distribution of p-values is compatible with the uniform distribution expected from the null hypothesis (see Appendix A of [27] for details). The test yields a background probability of 19.3%, which indicates that the distribution is consistent with no GW events being present.

As part of the analysis, we measured the sensitivity of the search to simulated GW signals as a function of amplitude. For this search, we simulate GWs from GRBs using circularly polarized sine-Gaussians (SGs) with quality factor $Q = 9$. These *ad hoc* waveforms model the GW emission of a rigidly rotating quadrupolar mass moment with a Gaussian-shaped amplitude evolution in time, and are the standard examples used for estimating the sensitivity of GW analyses to unmodeled, short-duration signals. We marginalize over systematic errors in sensitivity and phase between detectors by "jittering" the simulated waveforms in amplitude and central time before adding them to the detector data; the magnitude of the jitter is Gaussian-distributed with a width proportional to the calibration errors of each detector. Furthermore, for GRBs detected by the GBM, the sky positions of the simulated waveforms are distributed according to the systematic uncertainties of the GBM detector [73]. This sky position jittering is performed across the entire uncertainty region, and is not restricted to the axis of the linear search grid.

For each GRB we calculate the total amplitude in GW-induced strain that would result in a detection for 90% of the simulated signals; these 90% upper limits are given in Table I. In terms of GW strain amplitude, the median 90% upper limit for our GRB sample was 2.8×10^{-21} Hz$^{-1/2}$ for circularly-polarized SG signals at 500 Hz and 3.4×10^{-21} Hz$^{-1/2}$ at

1 kHz. Signals with frequencies below 300 Hz were typically only detectable at very large amplitude; this is due to the sensitivity of the GEO 600 detector, and to the choice of coherent cut thresholds, which were tuned to minimize the effect of nonstationary noise in GEO at low frequencies.

For a fixed GW emission energy, we calculate the lower limit on the distance to the GRB using:

$$D_{\text{excl}} = \sqrt{\frac{5}{2}}\sqrt{\frac{G}{\pi^2 c^3}}\frac{\sqrt{E_{\text{GW}}}}{f_0 h_{\text{rss}}} \tag{3}$$

where E_{GW} is the energy released by the GRB central engine in GWs, G is Newton's constant, f_0 is the central frequency of the rigid rotator model, and h_{rss} is the strain amplitude upper limit observed by the search. The factor of $\sqrt{5/2}$ arises from the beamed GW emission from a rotating quadrupolar system, viewed on-axis [88].

The distribution of exclusion distances for waveforms with central frequencies of 500 Hz and 1 kHz for the 129 GRBs in this search is shown in Sec. VI. The median exclusion distance for the 500 Hz and 1 kHz waveforms are 0.8 Mpc and 0.3 Mpc, respectively, where we have assumed the GRB central engine releases $E_{GW} = 10^{-2} M_\odot c^2$ total energy in GWs. The distance limits scale with the square root of the assumed emission energy, $E_{GW}^{1/2}$, and for a pessimistic assumption of $E_{GW} = 10^{-8} M_\odot c^2$ the median exclusion distance becomes 0.8 kpc at 500 Hz. For comparison, the GRB in our sample with the smallest observed redshift is GRB 080905A, with $z = 0.1218$ [89] or $D \simeq 590$ Mpc [90].

VI. SUMMARY AND FUTURE WORK

We have performed a search for unmodeled short-duration GW signals associated with 129 GRBs using data from the GEO 600, LIGO, and Virgo detectors. The search covered the frequency range 64 Hz–1792 Hz, and employed a new technique to analyze the large-uncertainty GRB sky localizations from the *Fermi* GBM. This search is the first to analyze GBM events for GW signals at frequencies above 500 Hz. We find no evidence for a GW candidate associated with any of the GRBs in this sample, and a statistical analysis shows no sign of a collective signature of subthreshold GW events. We have set upper limits on the GW strain at the Earth, assuming a fixed emission energy in GWs from the GRB central engine. In general, our upper limits only constrain plausible GW emission from GRBs for sources in the Local Group.

The LIGO and Virgo detectors are currently undergoing a major upgrade, implementing new techniques to greatly increase their sensitivity, and are expected to begin operations in 2015. An improvement on the upper limits presented here of a factor of twenty or more is likely once the advanced detectors reach their design sensitivity. Various population studies of GRBs with redshift measurements have predicted that the rate of coincident detection in GW observatories and gamma-ray observatories will be $\mathcal{O}(1)$ per year once advanced LIGO and Virgo reach their design sensitivities [91–96].

Our analysis demonstrates the potential for extending the search frequency band for GWs associated with GBM events above 1 kHz, and the reduced computational cost of this method will be useful for rapid triggered analyses of GBM events in the era of advanced GW detectors. In the event of a GW detection with signal content above 1 kHz, our search method can provide improved localization for GRBs with large uncertainties in sky location, which can be passed on to EM astronomers for follow-up using wide-field telescopes.

[1] P. Mészáros, Rep. Prog. Phys. **69,** 2259 (2006).
[2] R. W. Klebesadel, I. B. Strong, and R. A. Olson, Astrophys. J. **182,** L85 (1973).
[3] D. A. Frail *et al.*, Astrophys. J. **562,** L55 (2001).
[4] W. Fong *et al.*, Astrophys. J. **756,** 189 (2012).
[5] C. Kouveliotou, C. A. Meegan, G. J. Fishman, N. P. Bhat, M. S. Briggs, T. M. Koshut, W. S. Paciesas, and G. N. Pendleton, Astrophys. J. **413,** L101 (1993).
[6] T. J. Galama *et al.*, Nature (London) **395,** 670 (1998).
[7] J. S. Bloom *et al.*, Nature (London) **401,** 453 (1999).
[8] S. E. Woosley and J. S. Bloom, Annu. Rev. Astron. Astrophys. **44,** 507 (2006).
[9] D. Eichler, M. Livio, T. Piran, and D. N. Schramm, Nature (London) **340,** 126 (1989).
[10] R. Narayan, B. Paczynski, and T. Piran, Astrophys. J. **395,** L83 (1992).
[11] R. Mochkovitch, M. Hernanz, J. Isern, and X. Martin, Nature (London) **361,** 236 (1993).
[12] E. Nakar, Phys. Rep. **442,** 166 (2007).
[13] N. Gehrels, E. Ramirez-Ruiz, and D. B. Fox, Annu. Rev. Astron. Astrophys. **47,** 567 (2009).
[14] L. Rezzolla, B. Giacomazzo, L. Baiotti, J. Granot, C. Kouveliotou, and M. A. Aloy, Astrophys. J. Lett. **732,** L6 (2011).
[15] N. R. Tanvir, A. J. Levan, A. S. Fruchter, J. Hjorth, R. A. Hounsell, K. Wiersema, and R. L. Tunnicliffe, Nature (London) **500,** 547 (2013).
[16] E. Berger, W. Fong, and R. Chornock, Astrophys. J. Lett. **774,** L23 (2013).
[17] J. Abadie *et al.*, Astrophys. J. **755,** 2 (2012).
[18] B. P. Abbott *et al.*, Astrophys. J. **681,** 1419 (2008).
[19] A. M. Soderberg *et al.*, Nature (London) **442,** 1014 (2006).
[20] E. Liang, B. Zhang, F. Virgili, and Z. G. Dai, Astrophys. J. **662,** 1111 (2007).
[21] T. Le and C. D. Dermer, Astrophys. J. **661,** 394 (2007).
[22] R. Chapman, N. R. Tanvir, R. S. Priddey, and A. J. Levan, Mon. Not. R. Astron. Soc. Lett. **382,** L21 (2007).
[23] F. J Virgili, E.-W. Liang, and B. Zhang, Mon. Not. R. Astron. Soc. **392,** 91 (2009).
[24] E. J. Howell and D. M. Coward, Mon. Not. R. Astron. Soc. **428,** 167 (2013).
[25] B. Abbott *et al.*, Phys. Rev. D **77,** 062004 (2008).
[26] J. Abadie *et al.*, Astrophys. J. **715,** 1453 (2010).
[27] J. Abadie *et al.*, Astrophys. J. **760,** 12 (2012).
[28] J. Aasi *et al.*, Phys. Rev. D **88,** 122004 (2013).
[29] B. Abbott *et al.*, Phys. Rev. D **76,** 062003 (2007).
[30] B. P. Abbott *et al.*, Astrophys. J. Lett. **701,** L68 (2009).
[31] J. Abadie *et al.*, Astrophys. J. Lett. **734,** L35 (2011).
[32] J Aasi *et al.*, arXiv:1403.6639.
[33] A. Corsi, Proc. Int. Astron. Union **7,** 142 (2011).
[34] Edo Berger, Annu. Rev. Astron. Astrophys., **52** (2014).
[35] K. S. Thorne, in *Three Hundred Years of Gravitation*, edited by S. W. Hawking and W. Israel (Cambridge University Press, Cambridge, England, 1987), p. 330.
[36] K. Kiuchi, Y. Sekiguchi, M. Shibata, and K. Taniguchi, Phys. Rev. D **80,** 064037 (2009).
[37] Y. Sekiguchi, K. Kiuchi, K. Kyutoku, and M. Shibata, Phys. Rev. Lett. **107,** 051102 (2011).
[38] R. Oechslin and H. T. Janka, Phys. Rev. Lett. **99,** 121102 (2007).

[39] K. Hotokezaka, K. Kiuchi, K. Kyutoku, T. Muranushi, Y.-i Sekiguchi, M. Shibata, and K. Taniguchi, Phys. Rev. D, **88,** 044026 (2013).
[40] R. C. Duncan and C. Thompson, Astrophys. J. **392,** L9 (1992).
[41] N. R. Tanvir, R. Chapman, A. J. Levan, and R. S. Priddey, Nature (London) **438,** 991 (2005).
[42] K. Hurley *et al.*, Mon. Not. R. Astron. Soc. **403,** 342 (2010).
[43] E. P. Mazets, R. L. Aptekar, T. L. Cline, D. D. Frederiks, J. O. Goldsten, S. V. Golenetskii, K. Hurley, A. von Kienlin, and V. D. Pal'shin, Astrophys. J. **680,** 545 (2008).
[44] A. Corsi and B. J. Owen, Phys. Rev. D **83,** 104014 (2011).
[45] B. Zink, P. D. Lasky, and K. D. Kokkotas, Phys. Rev. D **85,** 024030 (2012).
[46] P. Lasky, B. Zink, and K. D. Kokkotas, arXiv:1203.3590.
[47] R. Ciolfi and L. Rezzolla, Mon. Not. R. Astron. Soc. **435,** L43 (2013).
[48] C. D. Ott, Classical Quantum Gravity **26,** 063001 (2009).
[49] C. D. Ott, A. Burrows, L. Dessart, and E. Livne, Phys. Rev. Lett. **96,** 201102 (2006).
[50] C. D. Ott, Classical Quantum Gravity **26,** 204015 (2009).
[51] C. L. Fryer, D. E. Holz, and S. A. Hughes, Astrophys. J. **565,** 430 (2002).
[52] S. Kobayashi and P. Mészáros, Astrophys. J. **589,** 861 (2003).
[53] A. L. Piro and E. Pfahl, Astrophys. J. **658,** 1173 (2007).
[54] A. L. Piro and E. Thrane, Astrophys. J. **761,** 63 (2012).
[55] M. H. van Putten, Phys. Rev. Lett. **87,** 091101 (2001).
[56] M. H. van Putten, A. Levinson, H. Lee, T. Regimbau, M. Punturo, and G. Harry, Phys. Rev. D **69,** 044007 (2004).
[57] M. Shibata and K. Taniguchi, Phys. Rev. D **77,** 084015 (2008).
[58] K. D. Kokkotas and B. Schmidt, Living Rev. Relativity **2,** 2 1999).
[59] M. Shibata and K. Taniguchi, Phys. Rev. D **73,** 064027 (2006).
[60] A. Bauswein, H.-T. Janka, K. Hebeler, and A. Schwenk, Phys. Rev. D **86,** 063001 (2012).
[61] H. Grote, Classical Quantum Gravity **25,** 114043 (2008).
[62] H. Grote *et al.*, Classical Quantum Gravity **27,** 084003 (2010).
[63] J. Abadie *et al.*, Nat. Phys. **7,** 962 (2011).
[64] H. Grote, K. Danzmann, K. L. Dooley, R. Schnabel, J. Slutsky, and H. Vahlbruch, Phys. Rev. Lett. **110,** 181101 (2013).
[65] B. P. Abbott *et al.*, Rep. Prog. Phys. **72,** 076901 (2009).
[66] T. Accadia *et al.*, JINST **7,** P03012 (2012).
[67] P. J. Sutton *et al.*, New J. Phys. **12,** 053034 (2010).
[68] C. Meegan *et al.*, Astrophys. J. **702,** 791 (2009).
[69] M. Was, P. J. Sutton, G. Jones, and I. Leonor, Phys. Rev. D **86,** 022003 (2012).
[70] A. C. Searle, P. J. Sutton, and M. Tinto, Classical Quantum Gravity **26,** 155017 (2009).
[71] M. S. Briggs, V. Connaughton, C. A. Meegan, C. Wilson-Hodge, M. Kippen, K. Hurley, C. Meegan, C. Kouveliotou, and N. Gehrels, AIP Conf. Proc. **1133,** 40 (2009).
[72] N. Gehrels *et al.*, Astrophys. J. **611,** 1005 (2004).
[73] V. Connaughton, GCN Report No. 11574, 2011.
[74] K. Hurley *et al.*, Astrophys. J. Suppl. Ser. **207,** 39 (2013).
[75] Leo P. Singer *et al.*, Astrophys. J. Lett. **776,** L34 (2013).

[76] J. Aasi *et al.*, arXiv:1304.0670.

[77] S. D. Barthelmy, Astron. Nachr. **329**, 340 (2008).

[78] A. von Kienlin *et al.*, Astrophys. J. Suppl. Ser. **211**, 13 (2014).

[79] C. Winkler *et al.*, Astron. Astrophys. **411**, L1 (2003).

[80] M. Feroci *et al.*, Nucl. Instrum. Methods Phys. Res., Sect. A **581**, 728 (2007).

[81] M. Matsuoka *et al.*, Publ. Astron. Soc. Jpn. **61**, 999 (2009).

[82] L. Blackburn *et al.*, Classical Quantum Gravity **25**, 184004 (2008).

[83] N. Christensen, Classical Quantum Gravity **27**, 194010 (2010).

[84] J. Aasi *et al.*, Classical Quantum Gravity **29**, 155002 (2012).

[85] J. R. Smith, T. Abbott, E. Hirose, N. Leroy, D. MacLeod, J. McIver, P. Saulson, and P. Shawhan, Classical Quantum Gravity **28**, 235005 (2011).

[86] T. Isogai, J. Phys. Conf. Ser. **243**, 012005 (2010).

[87] A. Cucchiara. GCN GRB Observation Report No. 5052, 2006.

[88] P. Sutton, arXiv:1304.0210.

[89] A. Rowlinson *et al.*, Mon. Not. R. Astron. Soc. **408**, 383 (2010).

[90] E. L. Wright, Publ. Astron. Soc. Pac. **118**, 1711 (2006).

[91] J. Abadie *et al.*, Classical Quantum Gravity **27**, 173001 (2010).

[92] A. Dietz, Astron. Astrophys. **529**, A97 (2011).

[93] I. Leonor, P. J. Sutton, R. Frey, G. Jones, S. Márka, and Z. Márka, Classical Quantum Gravity **26**, 204017 (2009).

[94] B. D. Metzger and E. Berger, Astrophys. J. **746**, 48 (2012).

[95] H.-Y. Chen and D. E. Holz, Phys. Rev. Lett. **111**, 181101 (2013).

[96] K. Siellez, M. Boer, and B. Gendre, Mon. Not. R. Astron. Soc. **437**, 649 (2014).